SICE Journal of Control, Measurement, and System Integration, Vol. 11, No. 1, pp. 014–024, January 2018

"Flyable" Guidance and Control Algorithms for Orbital Rendezvous Maneuver

Elisa CAPELLO [*,**], Fabrizio DABBENE [**], Giorgio GUGLIERI [*], and Elisabetta PUNTA [**]

Abstract : Rendezvous orbital maneuvers are planned operations which intend to make two spacecraft meet, while avoiding collisions. Aspects such as trajectory safety and robustness, as well as obstacle avoidance, are fundamental for the mission success. The aim of this paper is to provide an overview of some recent algorithms for guidance and control systems, and also their combined exploitation, which can provide significant enhancements. This overview focuses on those algorithms that are characterized by key selected features: the discussed schemes guarantee low computational effort, low fuel consumption, and high safety and robustness. Different experimental setups, which can be used to evaluate the performance of the considered algorithms, are also taken into account and presented.

Key Words : GNC systems, rendezvous maneuver, low computational effort, safety, obstacle avoidance.

1. Introduction

Rendezvous maneuvers represent a focal point for the success of spatial missions and explorations. Because of this, autonomous rendezvous and proximity operations have been significantly expanded in recent decades. Since the beginning of the space era, manned orbital rendezvous and docking maneuvers have been deeply studied and tested in the Gemini program [1], and further in the Apollo program [2], with the aim to dock two spacecraft to reach the Moon, to land on it, and to return the crew safely back to Earth.

More recently, automated mission to bring supplies to the International Space Station (ISS) are continuously flying, involving different type of spacecraft (ATV [3], HTV [4], Progress [5], Cygnus [6], and more). These spacecraft are unmanned, therefore an automated rendezvous mission has to be successfully completed with the support of a robust flight software.

Recent studies concern the use of unmanned spacecraft in orbital servicing mission and, in particular, the development of a robust flight software. This on-board software has to be designed so to manage unexpected events, such as environment disturbances and noise, and/or crossing of small objects. The present paper aims to provide an overview of some "flyable" guidance and control algorithms, able to be combined and to be implemented in real-time. The proposed approaches are designed to be as close as possible to "flyable" format, as required by EASA standards [7]. Indeed, the guidance navigation and control (GNC) system is implemented as space segment in which control systems and mission planners are considered. Some hardware constraints, such as limited updating frequency of both guidance and control algorithms, are also included.

[*] Department of Mechanical and Aerospace Engineering, Politecnico di Torino, Corso Duca degli Abruzzi 24, 10129 Torino, Italy

[**] CNR–IEIIT, Politecnico di Torino, Corso Duca degli Abruzzi 24, 10129 Torino, Italy
E-mail: elisa.capello@polito.it, fabrizio.dabbene@ieiit.cnr.it, giorgio.guglieri@polito.it, elisabetta.punta@ieiit.cnr.it
(Received October 2, 2017)

A recent survey on orbital dynamics and control was presented in [8], in which the relative dynamics equations and different rendezvous problems were analyzed. However, even if safety issues were presented in good details, no algorithms for GNC were included, and only a brief description of some automated control algorithms was included. Guidance and control algorithms for automatic rendezvous maneuver have been deeply discussed in the last ten years. More attention is usually dedicated to proximity maneuvers, as for instance in [9]. However, in general, disturbances or model uncertainties are not specifically discussed. In [10], the proximity maneuver is clearly described, in which the chaser is driven to a certain fixed position along the docking port and the relative attitude is synchronized for subsequent docking operations. External disturbances and model uncertainties are considered, but no trajectory tracking is included. A real scenario is analyzed in which both spacecraft are equipped with an on-board GNC system, to perform various rendezvous functions in an autonomous way and with extreme precision. The GNC system maintains and changes the vehicle's center of mass position and velocity, processing the sensor measurements, the computation of the flight trajectory, the navigation, the attitude and position control as well as the flight control and safety monitoring. An overview of the guidance and control algorithms is provided, focusing on real time applications and hardware constraints.

The aim of this paper is to provide an overview of some recent GNC systems, which are characterized by key features such as low computational effort, low fuel consumption, and high safety and robustness. Combinations of different guidance and control algorithms are also presented. For guidance algorithms, focusing on low computational effort and low fuel consumption and considering the results obtained in the work of Maclellan [11], feedback-based algorithms are selected. For this reason, in this paper, the well-known proportional navigation (PN) algorithm and the zero-effort-miss/zero-effort-velocity (ZEM/ZEV) theory are included, as they are suitable for on-board implementation. Moreover, in the same class of guidance laws, algorithms based on the theory of artificial potential fields can be also included. This last approach is con-

sidered for avoiding undesired collisions. Indeed, most of the literature on rendezvous assumes that the chaser may access any region of the maneuver in the space. However, many scenarios involve operations to be performed either near large space structures or, due to the increase of space debris, in proximity of obstacles [12]. Consequently, one of the essential requirements for automated rendezvous operations is the ability to maneuver in proximity of them, without collision. An obstacle avoidance algorithm for rendezvous maneuver is proposed in [13]. Two aspects can be considered as possible limitations of this approach: (i) an "ad hoc" method for guidance is proposed and (ii) the control algorithm works at high frequency. Starting from this work in [14] a method for spacecraft maneuver with obstacles is proposed, yet no control algorithms are considered and simplified dynamics is analyzed.

The paper is organized as follows. In Section 2 the considered maneuver is described and analyzed. Section 3 focuses on the spacecraft dynamics. The overview of some recent algorithms for guidance is provided in Section 4, while the control strategies are presented in Section 5. The experimental setups used to evaluate the performance of the considered algorithms are presented in Section 6. Finally, some concluding remarks are proposed in Section 7.

2. Problem Setup

As briefly discussed in the Introduction, in this paper we analyze a complete rendezvous maneuver as depicted in Fig. 1. The rendezvous mission is in general split into several major phases, as described e.g. in [15]: (i) the *homing phase*, where the chaser is driven form its starting orbit up to (or close to) the target orbit through a Hohmann transfer, (ii) the *closing phase*, i.e. a radial boost maneuver which brings the chaser closer to the target, within the same orbital plane, and (iii) the *final approach*, in which the chaser is driven by means of a controlled maneuver to reach and finally dock the target within a (cuboid) safety zone.

The whole maneuver starts at the waypoint S0 in Fig. 1, which represents the initial condition for the simulation, and in which the chaser is in a lower orbit with respect to the target, and it is located some kilometers far from it. If the maneuver is an impulsive (or quasi-impulsive) one, the resultant trajectory corresponds to the ideal *Hohmann transfer*. The next maneuver, from waypoint S2 to waypoint S3, is necessary to get closer to the target, and it is executed when the chaser is in the same orbit of the target. The position of the final point S3 depends on safety requirements, but it is usually located hundreds of meters far from the target position. The S3-S4 maneuver is a forced motion of the chaser to get the target, generally similar to a straight line approach. The simulation stops when the chaser is few meters far from the target. During the analyzed maneuver, the target is considered to lie in a fixed position, which is coincident with the origin of a local reference frame. The docking between the two spacecraft is not depicted because a multibody dynamics has usually to be considered to clearly understand the loads of contact.

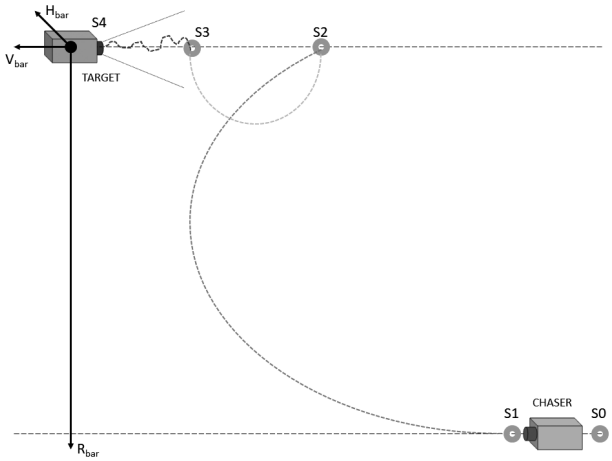

Fig. 1 Complete rendezvous and docking maneuver in Hill frame.

3. Spacecraft Dynamics

The spacecraft dynamics consists of the superposition of position dynamics and attitude dynamics. The position - or orbital - dynamics is based on propagation of equations of relative dynamics, usually known as *Hill's* or *Clohessy-Wiltshire* equations [15]. Attitude dynamics is formulated in the quaternion notation and it is propagated relative to the inertial Earth centered inertial reference frame (ECI) [16].

In this brief overview, we consider a classical spacecraft configuration, consisting of a thruster actuation system for position control, and an attitude control based on reaction wheels (RWs). The thrusters can exert mono-directional actions, that is, they can apply to the chaser thrusts of given magnitude and along fixed directions, which depend on how and where the thrusters have been assembled in the system (their orientations and application points). Three reaction wheels are considered for the attitude control. Spacecraft reaction wheels are typically between few kilograms to tens of kilograms of mass, and are driven by electric motors powered by the spacecraft electrical power supply. They are managed and controlled by the onboard attitude control computer. A reaction wheel (RW) actuator can be modeled as a brushless motor attached to a high-inertia flywheel which is free to spin along a fixed spacecraft axis. It produces a moment M_{RW}, causing the angular momentum to increase. For the representation of a realistic model of RW, a first order filter and a saturation on the maximum-minimum torque assigned by the RW are also included in the actuator model.

For a complete description of the derivation of Hill's equations from inertial equations, the reader is referred to [15]. Hill's equations describe the relative motion between two objects orbiting in slightly different orbits and are computed with respect to the origin of a local-vertical-local-horizontal (LVLH) reference frame (Fig. 2), usually coincident with the center of mass of the target. The following assumptions are in general formulated:

1. The orbit of the reference object must be circular. However, a modified formulation of Hill's equations for non circular orbits can be found in literature [17].

2. The validity of the approximation of Hill's equations is limited to few kilometers of distance along each axis. Introduction of curvilinear x and y coordinates may partially extend the validity of Hill's equations mitigating position error due to the curvature of Earth. Curvilinear coordinates are not considered here for the sake of simplicity.

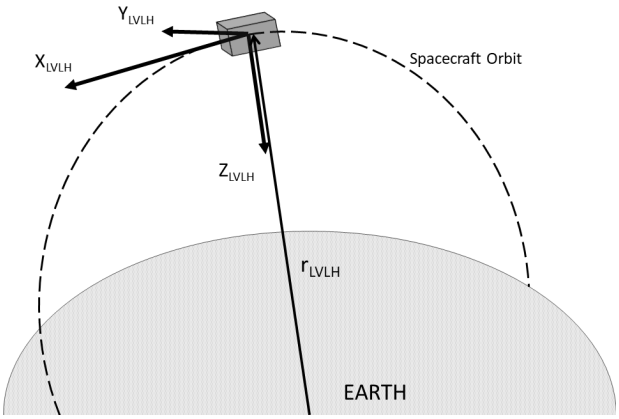

Fig. 2 LVLH frame definition.

In the literature, the coordinates x_{LVLH}, y_{LVLH} and z_{LVLH} are sometimes referred to as *V-bar*, *H-bar* and *R-bar*, respectively. Hill's equations for circular orbit, which are time-integrated to propagate the relative orbit [15], are as follows

$$\begin{aligned}\ddot{x} &= \frac{F_x}{m_c} + 2\omega_0\dot{z},\\ \ddot{y} &= \frac{F_y}{m_c} - \omega_0 y,\\ \ddot{z} &= \frac{F_z}{m_c} - 2\omega_0\dot{x} + 3\omega_0^2 z,\end{aligned} \tag{1}$$

where $\ddot{x}$, $\ddot{y}$ and $\ddot{z}$ are accelerations, $\dot{x}$, $\dot{y}$ and $\dot{z}$ are velocities, x, y, and z are positions. All variables are computed with respect to LVLH frame. The term ω_0 denotes the orbital angular velocity of the reference LVLH frame, and m_c is the mass of the spacecraft. The total force acting on the spacecraft $F = [F_x, F_y, F_z]^T \in \mathbb{R}^3$ includes both force due to the thrusters system and external disturbances. Hence, we have

$$F = F_{\text{thr}} + F_{\text{ext}}, \tag{2}$$

where $F_{\text{thr}} \in \mathbb{R}^3$ is the thruster force and $F_{\text{ext}} \in \mathbb{R}^3$ is the external disturbances perturbation, both expressed in LVLH frame. The main disturbance affecting low Earth orbit (LEO) maneuvers, in terms of magnitude, is the drag force due to the residual atmosphere. The oblateness of Earth, which affects orbital parameters of the reference object and the relative position dynamics, and the solar radiation pressure are one order of magnitude smaller than the drag.

We remark that the RCS model is defined in Body frame, so, to obtain the thrust force in the LVLH frame, a rotation has to be applied, that is

$$F_{\text{thr}} = R_{LVLHb}(\phi, \theta, \psi) F^b_{\text{thr}},$$

where $F^b_{\text{thr}} \in \mathbb{R}^3$ is the thrust force expressed in Body frame and $R_{LVLHb}(\phi, \theta, \psi)$ is the rotation matrix from Body frame to LVLH frame.

The magnitude of the thrust produced by each thruster is affected by bias and random errors, as well as the thrust direction is affected by both type of errors. Hence, the magnitude of each thruster i can be expressed as

$$F^i_{mag} = F^i_{nom} + \Delta F^i_{bias} + \Delta F^i_{noise},$$

where F^i_{nom} is the nominal thrust , ΔF^i_{bias} is the bias thrust error and ΔF^i_{noise} is the thrust noise. Both these contributions are different for each thruster. A similar formulation can be used to model the thrust direction:

$$f^i = [R^i_{rand}(\delta_{rand}, \epsilon_{rand}, \zeta_{rand})][R^i_{bias}(\delta_{bias}, \epsilon_{bias}, \zeta_{bias})] f^i_{nom},$$

where $f^i \in \mathbb{R}^3$ is the unitary vector representing the thrust direction of thruster i affected by errors, $f^i_{nom} \in \mathbb{R}^3$ is the unitary vector representing the nominal thrust direction of thruster i, $R^i_{bias}(\delta_{bias}, \epsilon_{bias}, \zeta_{bias})$ is the rotation matrix relative the nominal direction of thruster i computed with bias angles and $R^i_{rand}(\delta_{rand}, \epsilon_{rand}, \zeta_{rand})$ is the rotation matrix relative to the nominal direction of thruster i computed with random angles. Finally, the thrust provided by thruster i expressed in Body frame can be computed as

$$F^i = [f^i] F^i_{mag}, \tag{3}$$

where $F^i \in \mathbb{R}^3$ is the force provided by thruster i. Hence, the total force provided by the RCS is expressed as

$$F^b_{\text{thr}} = \sum_{i=1}^{N_{\text{thr}}} F^i,$$

with N_{thr} number of thrusters.

As previously mentioned, the attitude dynamics is propagated using the quaternion formulation. Angular velocity in body frame can thus be obtained by

$$\dot{\omega}_B = I^{-1}(M_B - \omega_B \times (I\omega_B + I_{\text{RW}}\omega_{\text{RW}})),$$

where $\dot{\omega}_B \in \mathbb{R}^3$ is the angular acceleration with respect to Body frame, $I \in \mathbb{R}^{3,3}$ is the inertia tensor, $M_B \in \mathbb{R}^3$ is the total torque acting on the spacecraft, $\omega_B \in \mathbb{R}^3$ is the angular velocity of the spacecraft, $I_{\text{RW}} \in \mathbb{R}^{3,3}$ is the inertia of the reaction wheels system and $\omega_{\text{RW}} \in \mathbb{R}^3$ is the angular velocity of the reaction wheels system. The total torque acting on the spacecraft is the sum of different elements

$$M_B = M_{\text{thr}} + \Delta M_{\text{ex}} + M_{\text{RW}},$$

where $M_{\text{thr}} \in \mathbb{R}^3$ is the torque due to the RCS, $\Delta M_{\text{ex}} \in \mathbb{R}^3$ is the torque due to external disturbances and $M_{\text{RW}} \in \mathbb{R}^3$ is the torque generated by the reaction wheels system. The torque generated by the thrusters system is obtained by

$$M_{\text{thr}} = \sum_{i=1}^{N_{thr}} r^i_{thr} \times F^i,$$

where r^i_{thr} is the position of the thruster i relative to the center of mass and F^i is defined by (3). The external torque affecting the attitude dynamics of the spacecraft is mainly due to the gravity gradient torque. Other torque disturbances such as aerodynamic torque and torque due to the solar radiation are one order of magnitude smaller than the gravitational moment.

For the quaternions, the following notation can also be used (useful for the attitude control definition)

$$\dot{q} = \tfrac{1}{2}\Sigma(q)\omega_B, \tag{4}$$

where $q = [q_1\ q_2\ q_3\ q_4]^T \in \mathbb{R}^4$ is again the vector of quaternions and $\Sigma(q) \in \mathbb{R}^{3,4}$ is the quaternion matrix, defined as

$$\Sigma(q) = \begin{bmatrix} q_4 I_3 + Q_{13} \\ -q_{13}^T \end{bmatrix}, \tag{5}$$

where $q_4 \in \mathbb{R}$ is the quaternion scalar component, $q_{13} \in \mathbb{R}^3$ is the vector of the first three components of the vector q and $Q_{13} \in \mathbb{R}^{3,3}$ is the skew-symmetric matrix

$$Q_{13} = \begin{bmatrix} 0 & -q_3 & q_2 \\ q_3 & 0 & -q_1 \\ -q_2 & q_1 & 0 \end{bmatrix}.$$

The attitude is propagated with respect to the Earth centered inertial (ECI) frame.

4. Guidance Algorithms

The main goal of a guidance scheme is to obtain a planned trajectory for the spacecraft translational dynamics, and to assign desired attitude for rotational dynamics. Thus a guidance algorithm defines the desired variations that constitute the inputs of the control system, whose design is discussed in Section 5. In layman's terms, *the guidance law defines the trajectory that the spacecraft has to follow to reach the desired final position*.

Guidance algorithms may be divided in two classes: (i) predictive guidance schemes, and (ii) feedback-based guidance laws, which also use on-off pulses. The first class includes the following guidance laws (i) Lambert guidance [18] and (ii) time-varying state transition matrix (STM) guidance [19]. Other guidance laws, based on the same theory, have been derived to follow a known path to the target, for example the work [20], or to intercept an asteroid with terminal velocity direction constraints [21]. As pointed out in the Introduction, in this paper we do not discuss this first class of laws, and concentrate on feedback-based guidance algorithms. As discussed in [11], this class of guidance laws can guarantee safety robustness and low computational effort, thus resulting to be well suitable for real-time applications.

Different feedback-based approaches have been considered in the last years. The following guidance algorithms are analyzed in this paper.

a. Proportional navigation (PN) algorithm, which issues acceleration commands perpendicular to the instantaneous chaser-target line-of-sight (LOS), that are proportional to the LOS rate and closing velocity [22].

b. ZEM/ZEV optimal feedback guidance laws are usually used for asteroid intercept and rendezvous missions, through the definition of an acceleration command related to terminal velocity direction or magnitude requirements, when the gravitational field could be assumed as an explicit function of time [23],[24].

c. In the same class of guidance law, algorithms based on artificial potencial field (APF) theory can be considered, to handle model uncertainties and obstacles [25].

The first two proposed guidance algorithms (PN and ZEM/ZEV) are usually used for asteroid maneuver. However, in [26] the authors proposed to employ these algorithms for a final cone-approach maneuver, in which strict requirements in terms of positions and speeds are required. The novelty of the approach proposed in [26] was to test and combine guidance and control algorithms, usually not implemented for rendezvous maneuver, and to validate these "non-standard" combinations, in order to be translated into a numerical algorithm (i.e. to be implemented on board). Main results are presented and discussed in [26] and extensive simulations are performed to prove the efficiency of the selected guidance algorithms.

4.1 Proportional Navigation

The first guidance algorithm we discuss is the so-called proportional navigation (PN) guidance. The PN takes into account the line-of sight angle λ, which represents the angle between the actual chaser velocity vector and the chaser-target connection line. This algorithm tries to drive the related LOS rate to zero though the application of an acceleration command, perpendicular to the LOS direction. The PN guidance law is expressed as

$$a = nV_c\dot{\lambda}, \tag{6}$$

where $a \in \mathbb{R}^3$ is the required control acceleration, V_c is the chaser closing velocity with respect to the target, $\dot{\lambda}$ is the LOS rate, and n is a designer-tunable parameter that represents the effective navigation gain, typically chosen between 3 and 5, where larger values are used when the robustness has to prevail on disturbances [22]. In terms of orbital components in LVLH frame, we have

$$a_x = -nV_c\dot{\lambda}\sin\lambda, \tag{7}$$

$$a_z = nV_c\dot{\lambda}\cos\lambda. \tag{8}$$

The other two terms can be evaluated as

$$V_c = -\dot{r} = -\frac{(x\dot{x} - z\dot{z})}{r}, \tag{9}$$

$$\dot{\lambda} = \frac{(x\dot{z} - z\dot{x})}{r^2}, \tag{10}$$

with x and z positions with respect to LVLH frame, and $\dot{x}$ and $\dot{z}$ velocities. This guidance law is usually used in missile applications as an interceptor guidance law because it is very easy to implement and is very effective, as described in Zarchan [22].

4.2 Zero-Effort-Miss/Zero-Effort-Velocity

The ZEM term is the distance between the chaser and the target considering that the target is moving along a pre-defined path (known). It is assumed that no additional control action is provided. The ZEV term can be defined as the end-of mission velocity offset with no acceleration applied. In particular, in order to get these two terms, the dynamic equation of motion with no control acceleration has to be integrated, leading to

$$\text{ZEV} = v_f - \left[v + \int_t^{t_f} g(\tau)d\tau\right], \tag{11}$$

$$\text{ZEM} = r_f - \left[vt_{go} + \int_t^{t_f} (t_f - \tau)g(\tau)d\tau\right], \tag{12}$$

where $r_f \in \mathbb{R}^3$ and $v_f \in \mathbb{R}^3$ are the desired final position and velocity, t_{go} represents the time-to-go, i.e., the mission flight time necessary to achieve the target, usually evaluated with respect to relative position and velocity, and t_f is the final maneuver time. The term $g(\tau)$ denotes the acceleration gravity evaluated at time τ. Starting from these terms, the optimal control law with specified terminal position and velocity, associated to the target, is obtained in a general formulation as

$$a = \frac{6}{t_{go}^2}\mathrm{ZEM} - \frac{2}{\mathrm{t_{go}}}\mathrm{ZEV}, \tag{13}$$

where $a \in \mathbb{R}^3$ is the required control acceleration, $t_{go} = t_f - t$ is the time-to-go.

4.3 Modified Zero-Effort-Miss/Zero-Effort-Velocity

Starting from the general formulation of the ZEM/ZEV, a novel approach for the development of a GNC algorithm was proposed in [27] for low Earth orbit environment. The idea is to modify the classical ZEM/ZEV (as in [23],[24] and in Section 4.2), starting from an ideal trajectory and considering the ideal positions and velocities as final parameters. The goal is to avoid high acceleration commands.

As extensively discussed in [27], the modified ZEM/ZEV is very effective in driving a chaser spacecraft along a complete rendezvous and docking maneuver, even in the presence of disturbances due to external perturbations and to the imperfections of the actuation system.

Expanding the ZEM and ZEV terms in (11) and (12), we obtain

$$\begin{aligned} \mathrm{ZEM} &= \mathrm{r_f} - \tilde{\mathrm{r}}_\mathrm{f}, \\ \mathrm{ZEV} &= \mathrm{v_f} - \tilde{\mathrm{v}}_\mathrm{f}, \end{aligned} \tag{14}$$

where $r_f \in \mathbb{R}^3$ and $v_f \in \mathbb{R}^3$ are the desired final position and velocity as in (11)–(12), while $\tilde{r}_f \in \mathbb{R}^3$ and $\tilde{v}_f \in \mathbb{R}^3$ are the predicted position and velocity at $t = t_{go}$.

Choosing properly the final maneuver time t_f is not a trivial task: indeed a bad choice of t_f could cause extremely high values of the command acceleration, since $1/t_{go}$ tends to infinity as the time t increases.

The proposed approach is as follows. Instead of computing the final position and velocity vectors required as terminal conditions of the entire maneuver, the ZEM/ZEV terms in Eq. (14) are implemented as positions and velocities that the spacecraft should maintain while it is following an ideal maneuver.

In order to generate the ideal trajectory that the chaser shall follow to complete a phase of the rendezvous and docking maneuver, the Clohessy-Wiltshire equations have to be propagated forward with time from a starting time t_0 to a finish time t_f which varies according to the specific maneuver.

As depicted in Fig. 1 the whole maneuver is composed by different phases (Hohmann, R-bar pulse (Radial Boost), etc.). This means that the initial conditions of the generated ideal maneuver have to be changed when a different phase is considered [15]. As a consequence, the GNC software has to compute the coefficients of Eq. (14) using different initial conditions for each phase before starting running the ZEM/ZEV algorithm and generate the guidance law.

To compute ZEM and ZEV errors, it is required to estimate the predicted terminal conditions, which, in this proposed approach, are the position $\tilde{r}_f$ and the velocity $\tilde{v}_f$ computed forward in time by Δt.

This means that the new coefficients $\tilde{r}_f \in \mathbb{R}^3$ and $\tilde{v}_f \in \mathbb{R}^3$ are computed during each phase of the simulation. Applying this approach, as discussed in [27], the overall control law is less sensitive to the time-to-go t_{go}, as compared to what usually happens in the classical ZEM/ZEV approach. Moreover, the use of a short-term prediction horizon Δt allows computing predicted position and velocity with small errors even in the case of high nonlinear systems.

The complete formulation is presented in [27], where simulation results are presented, confirming that this algorithm is promising in terms of disturbance rejection, robustness and performance, providing strict compliance of terminal conditions with nominal reference states, as a major achievement of ZEM/ZEV algorithm implementation. The authors of [27] combine this guidance design with a classical linear quadratic regulator (LQR) attitude control, discussed in Section 5.

4.4 Artificial Potential Fields

Since one of the essential requirement for automated rendezvous maneuver is the ability to reach the target and to maneuver in proximity of obstacles, as discussed in the Introduction, the motivation of using APFs is to provide an analytical method to reach the target in a safe way.

The main idea of the artificial potential field theory is to construct a potential field with a gradient acting attractive toward the goal and repellent from obstacles (see Fig. 3). The desired velocity and attitude are defined by the APF algorithm with the aim to avoid obstacles. This interpretation of the gradient was proposed in [25], in which a sliding mode control strategy for tracking the gradient due to artificial potential field is described.

As discussed in details in [28], the advantage of the use of the artificial potential fields for a rendezvous maneuver is twofold: (i) an autonomous way for the desired path is designed with a low computational effort, and (ii) an online update of the path is guaranteed, in particular in the the presence of obstacles. The algorithm, here described, can be combined with a sliding mode control (SMC), including both position and attitude dynamics. In [29] the problem of controlling an autonomous wheeled vehicle with an SMC is proposed, including collision avoidance.

The rendezvous maneuver requires, in presence of obstacles, to be performed completely autonomously with only sensors and on-board GC algorithms. Moreover, the GC algorithms must be able to simultaneously achieve a series of translational maneuvers in presence of external disturbances and uncertainties. The potential field method can produce low impulsive fuel and can be implemented on-line with a low computational effort. At each time step, the artificial potential field algorithm generates the desired velocity and orientation, required to reach the target. The desired vectors are generated considering the end of each maneuver as a minimum and the obstacle as a maximum and are not known a priori (no predetermined trajectory is considered).

A paraboloid artificial potential field is considered and the speed of the chaser decreases, as it approaches the goal (target

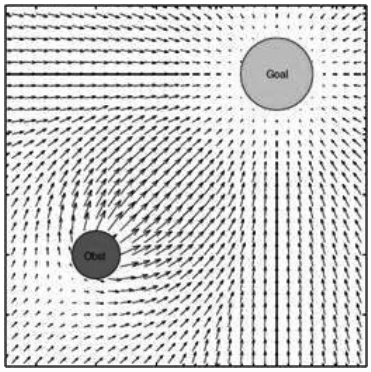

Fig. 3 Attractive and repulsive potential field [30].

spacecraft).

The attractive potential field is evaluated as

$$U_a(x) = \tfrac{1}{2} k_a \|e(x)\|^2, \tag{15}$$

$$f_a(\mathrm{x}) = -\nabla \mathrm{U_a(x)}, \tag{16}$$

where k_a defines how fast the attractive gradient goes to the goal, $e(\mathrm{x})$ is the error in position in which $\mathrm{x} = (x, y, z)^T \in \mathbb{R}^3$ is the position in LVLH frame. The attractive force is due to the gradient of the artificial potential field. To assign the direction of the desired speed, a unit vector of the potential field is evaluated

$$E_U = \frac{f_a(\mathrm{x})}{\| \nabla U_a(\mathrm{x}) \|},$$

thus the desired speed $\dot{x}_d \in \mathbb{R}^3$ is

$$\dot{x}_d = \dot{x}_{d,max} E_U,$$

where $\dot{x}_{d,max}$ is the maximum speed to perform the maneuver, which is scalar and equal along the three axes.

To avoid the obstacles, a repulsive potential field is defined, one for each obstacle ($i = 1, \dots N_{obs}$ with N_{obs} number of obstacles)

$$U_{r,i}(\mathrm{x}) = \begin{cases} \frac{k_{r,i}}{\gamma} \left(\frac{1}{\eta_i(\mathrm{x})} - \frac{1}{\eta_{0,i}(\mathrm{x})} \right)^{\gamma} & \text{if } \eta_i(\mathrm{x}) \le \eta_{0,\mathrm{i}}(\mathrm{x}), \\ 0 & \text{if } \eta_i(\mathrm{x}) > \eta_{0,\mathrm{i}}(\mathrm{x}), \end{cases} \tag{17}$$

where $k_{r,i}$ is the gain related to the repulsive field, $\gamma = 2$ is defined for hyperbolic field, $\eta_i(\mathrm{x}) = \min_{\mathrm{x_{obs}} \in \mathrm{CO^i}} \|\mathrm{x} - \mathrm{x_{obs}}\|$, $\mathrm{x_{obs}} \in \mathbb{R}^3$ is the obstacle position, and $\eta_{0,i}(\mathrm{x})$ is the safety radius. CO^i is the convex set of obstacles. The repulsive field is defined for each obstacle that is assumed convex. As before, the repulsive force is

$$f_{r,i}(\mathrm{x}) = \begin{cases} \frac{k_{r,i}}{\eta_i^2(\mathrm{x})} \left(\frac{1}{\eta_i(\mathrm{x})} - \frac{1}{\eta_{0,i}(\mathrm{x})} \right)^{\gamma - 1} \nabla \eta_i(\mathrm{x}) & \text{if } \eta_i(\mathrm{x}) \le \eta_{0,\mathrm{i}}(\mathrm{x}), \\ 0 & \text{if } \eta_i(\mathrm{x}) > \eta_{0,\mathrm{i}}(\mathrm{x}). \end{cases} \tag{18}$$

As discussed, the radius $\eta_{0,i}$ for $i = 1, \dots N_{obs}$ is the safety radius, and it means that the chaser senses the obstacle when it is $\eta_{0,i}$ m far from the obstacle. The applied artificial potential field is the sum of the attractive and repulsive parts (see Fig. 4),

$$U_t(\mathrm{x}) = U_a(\mathrm{x}) + \sum_{i=1}^{N_{obs}} U_{r,i},$$

and the total vector indicating the motion direction opposite of the artificial potential field is

$$E(x) = -\nabla U_t(\mathrm{x}),$$

with $E(x) \in \mathbb{R}^3$.

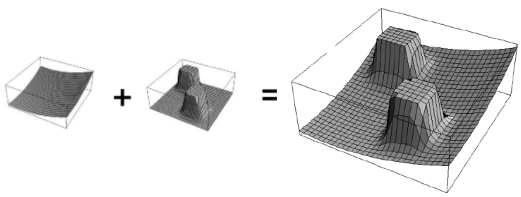

Fig. 4 Total artificial potential fields [31].

5. Control Algorithms

The aim of the control strategy is twofold: i) the controller must guarantee that the chaser tracks the specified position of the target while ii) the attitude stability is maintained. These goals must be reached despite the uncertainties due to the environmental disturbances and due to the actuation system, the performance of which is subject to physical constraints related to their feasible switching frequency and intensity of the thrusts. Concerning the attitude stabilization, it should be remarked that it represents a problem of particular importance for spacecraft, since it is fundamental for enforcing precision, and also for guidance, as short propulsive maneuvers must be executed with extremely accurate alignment [32].

Different control techniques have been proposed in the literature for automated rendezvous and docking, including $\mathcal{H}_\infty$ control [33], Riccati equation techniques [34],[35], graph theory [36], feedback-linearization-based approach [37]. In the last years, special attention has been reserved to the adoption of model predictive control (MPC) as control techniques for autonomous rendezvous and docking (ARVD), due to its capability of dealing with the constraints that typically characterize this maneuver, both in terms of relative position and velocity. Moreover, MPC offers a certain degree of robustness to system uncertainties due to its receding-horizon implementation. One example related to a space system is the linear quadratic MPC (LQ-MPC) adopted to enforce thrust magnitude limitation, line of sight (LOS) constraints, and velocity constraints for soft docking in [38]. In [39] a low-complexity MPC scheme for three degree-of-freedom (DoF) spacecraft system is developed for the low-thrust rendezvous and proximity operations. In the proposed approach, the thrust profile is parametrized with a set of Laguerre functions. In [40] a nonlinear model of spacecraft and cone constraints are described, considering a constant attitude variation.

However, it should be remarked that most of these approaches do not take into specific account orbital perturbations, disturbances, and model errors. Motivated by these considerations, in this overview we focus our attention on the following control approaches:

a. Sliding mode controllers (SMC) were implemented both for the position and the attitude control. The authors of [41] and [42] proposed SMC algorithms, easily implementable on-board and able to guarantee good performance even if hardware constraints and actuator dynamics are taken into account.

b. Tube-based model predictive control is proposed in [43], in which the results show that it can be implemented on-board for the real-time control of the final phase of a rendezvous and docking (RVD) maneuver.

c. Stochastic model predictive control (SMPC) is introduced in [44], starting from the work of the authors in [45],[46]. A sampling-based SMPC approach is proposed in [44] to control the proximity phase of an ARVD.

As already discussed, the proposed control algorithms are suitable to be combined with the described guidance laws, to obtain the desired performance, with a minimum fuel consumption and with an optimal tracking, including real-time applications.

5.1 Linear Quadratic Regulator

In this section, before discussing more advanced techniques, we briefly review the classical linear quadratic regulator (LQR), which is frequently considered for attitude stabilization [47]–[50]. In this case, the task of the control function is to provide the force and torque commands which will be executed by the reaction wheels to correct the deviations of the actual state vector from the nominal one, compensating also the effects of disturbances and errors. In particular, in [26],[27], LQR control is proved effective when combined to the described guidance laws. We need to remark that, for the design of an LQR, a linearized dynamic model needs to be considered, in which gyroscopic torque due to RW is neglected, as detailed in [26],[27]. That is, we consider a linear system of the form

$$\dot{x} = Ax + Bu, \tag{19}$$

where $x \in \mathbb{R}^3$ and $u \in \mathbb{R}^3$ represent respectively the state and the input vectors at time t. As well known, the design of an LQR controller consists in generating a control torque equal to

$$u = -Kx, \tag{20}$$

where x is the state and $K = R^{-1}B^T P$ is the static gain obtained by the solution P of the associated algebraic Riccati equation (ARE):

$$PA + A^T P - PBR^{-1}B^T P + Q = 0, \tag{21}$$

where Q and R are weighting matrices of suitable dimensions. The corresponding control action minimizes the classical quadratic cost function

$$J(x,u) = \int_0^\infty (x^T Qx + u^T Ru)dt. \tag{22}$$

5.2 Sliding Mode Controllers

The authors of [41] proposed an approach based on the design of two controllers: (1) a first-order SMC for position tracking and (2) a super-twisting (STW) second-order SMC for attitude stability, in which the mutual influence is taken into account by the introduction of additional disturbances. Key features and the feasibility of the approach proposed in [41] are in terms of i) fuel consumption, ii) robustness to model uncertainty and exogenous disturbances, and iii) fault tolerance.

Sliding mode methods provide controllers which are robust under large uncertainties. SMC can counteract uncertainties and disturbances, if the perturbations affecting the system are matched and bounded (first order SMC) [51] or smooth matched disturbances with bounded gradient (second order SMC) [52],[53]. The case of unmatched bounded disturbances is more involved. Nevertheless, under some posed conditions, it can be dealt with by suitably designed sliding mode control strategies [54]–[56].

For the position tracking, in [41] a first order sliding mode is designed, motivated by the intrinsic nature of the thrusters, which cannot provide continuously modulated thrusts, but can only be switched on and off. Indeed, the limited switching frequencies of the thrusters already pose serious feasibility issues to the implementation of a first order sliding mode control, considering both the fuel consumption and the capability to guarantee that the system trajectories reach and maintain a motion on the desired sliding manifold. In order to overcome these problems, the design of the control strategy is divided into two stages, which are identified mainly based on the chaser distance from the target and on different control switching parameters.

The control vector u is designed according to the following first order sliding mode control law

$$u_x = -B_x^{-1} K \mathrm{sgn}(\sigma_x), \tag{23}$$

where $B_x^{-1} = m_c(t)I_3$, $K = nT_{max}$, being $n = 2$ to reflect that two thrusters are switched on simultaneously, and σ_x represents the designed sliding output. In general, the control gain K in (23) must guarantee that the sliding motion on the desired sliding manifold is reached and maintained. The sliding output σ_x, which is the switching function in the controller (23), is

$$\sigma_x = (\dot{x} - \dot{x}_d) + c_x(x - x_d), \tag{24}$$

where $\dot{x}_d$ and x_d are the vectors of the desired speed and the desired positions, respectively. The vectors of position $x = [\mathrm{x}, \mathrm{y}, \mathrm{z}]^T$ and speed $\dot{x} = [\dot{\mathrm{x}}, \dot{\mathrm{y}}, \dot{\mathrm{z}}]^T$ are measured at each time step. The constant c_x is chosen positive. The desired sliding surface is $\sigma_x = 0$.

For the tracking control problem of the attitude of the chaser a second order sliding mode (2-sliding mode) algorithm, known as super-twisting (STW) [53], is analyzed in [41]. The STW algorithm designs a continuous control law, which steers to zero in finite time both the sliding output and its first time derivative, in the presence of smooth matched disturbances with bounded gradient for which a bound is assumed to be known. The STW algorithm contains a term which is obtained as the integral of a discontinuous component. The chattering is not eliminated, yet strongly attenuated.

The input u_ω is defined in accordance to the STW algorithm [53] as follows:

$$\begin{aligned} u_\omega &= -\lambda|\sigma_\omega|^{\frac{1}{2}}\mathrm{sgn}(\sigma_\omega) + v_\omega\,, \\ \dot{v}_\omega &= \begin{cases} -u_\omega & \text{if } |u_\omega| > U_M\,, \\ -\alpha\mathrm{sgn}(\sigma_\omega) & \text{if } |u_\omega| \le U_M\,, \end{cases} \end{aligned} \tag{25}$$

where the control parameters λ, α, and U_M have to be chosen as specified in [53].

The sliding output for the super-twisting controller is defined as

$$\sigma_\omega = \omega_B + C_\omega \delta q_{13}, \tag{26}$$

with $C_\omega \in \mathbb{R}^{3,3}$ positive definite matrix. The vector δq_{13} is evaluated starting from the desired attitude vector $q_d = [0\,0\,0\,1]^T$, that means that the LVLH and body frames are aligned

$$\delta q_{13} = \Sigma^T(q_d)q \tag{27}$$

where $\Sigma(q_d)$ is defined from the matrix $\Sigma(q)$ (Eq. (5)) in which the desired quaternion vector $q_d = [0, 0, 0, 1]^T$ is included.

More details about the formulation and the results of the proposed maneuver are in [41]. Simulation analysis demonstrates good performance of the controller, even when the switching frequencies of the thrusters are low. Future directions of research will be focused on using second-order sliding-mode algorithms with adaptive gains for the attitude control. They will be mostly focused on exploiting advanced simplex SMC strategies, as introduced in [42], with the aim of deriving better shooting strategies and of developing position tracking systems that could be configurable in case of failures.

5.3 Tube-Based Model Predictive Control

A very promising control strategy for the control of the rendezvous maneuver is that based on model predictive control (MPC). In particular, since we are interested in approaches able to cope with real-world situations, we concentrate here on robust MPC. In [43], the authors present an analysis of the real-time performance of tube-based robust MPC (TRMPC) [57]–[59] able to handle uncertainties due to external disturbances and additive noise. This novel approach focuses on two main goals: (i) to provide robustness to additive disturbances and (ii) to maintain the computational efficiency of a classical MPC. To this end, as discussed in [43],[57], this algorithm is split in two parts: (i) an offline evaluation of the constraints to ensure that the uncertain future trajectories lie in sequence of sets, known as *tubes*, and (ii) the online MPC scheme applied to the nominal trajectories, representing the center of the tube itself as in [57].

Let consider a generic discrete-time model of the form

$$\mathrm{x}_{k+1} = A_d \mathrm{x}_k + B_d \mathrm{u}_k + B_{w_d} \mathrm{w}_k, \tag{28}$$

where the noise is a realization of a stochastic process, each one being an independent and identically distributed (i.i.d.), zero-mean random variable, with bounded and convex support $\mathbb{W} \in \mathbb{R}^n$, containing the origin in its interior.
The system is subject to hard constraints on the state and input of the form

$$\mathrm{x} \in \mathbb{X}, \quad \mathrm{u} \in \mathbb{U}, \tag{29}$$

where $\mathbb{X}$ and $\mathbb{U}$ are polytopes. To solve the control problem, the algorithm proposed in [58] is repeatedly solved to minimize the quadratic cost $J_N(\mathrm{x}, \mathbf{u})$ at the current time k, where $\mathbf{u}$ is the control sequence.

Due to the presence of a bounded and persistent unknown disturbance w, the state of the system $\mathrm{x}_{i|k}$ can be split into a nominal part, $\mathrm{z}_{i|k}$, and an error part, $\mathrm{e}_{i|k}$, which represents the deviation of the actual state $\mathrm{x}_{i|k}$ with respect to the nominal one. We apply the following feedback policy

$$\mathrm{u}_{i|k} = \mathrm{v}_{i|k} + K(\mathrm{x}_{i|k} - \mathrm{z}_{i|k}), \tag{30}$$

where $\mathrm{v}_{i|k}$ is the new control input, and the matrix K is chosen so that $A_{d_K} = A_d + B_d K$ is Schur stable. Then, the corresponding nominal and error dynamics can be described respectively by

$$\mathrm{z}_{i+1|k} = A_d \mathrm{z}_{i|k} + B_d \mathrm{v}_{i|k}, \quad \mathrm{z}_{0|k} = \mathrm{x}_{0|k}, \tag{31}$$

$$\mathrm{e}_{i+1|k} = A_{d_K} \mathrm{e}_{i|k} + B_{w_d} \mathrm{w}_{i|k}, \quad \mathrm{e}_{0|k} = 0. \tag{32}$$

Hence, the finite horizon optimal quadratic cost $J_N(\mathrm{x}, \mathbf{u})$ can be re-defined in terms of nominal state z_k and control input sequence $\mathbf{v}_k$ as

$$J_N(\mathrm{z}_k, \mathbf{v}_k) = \sum_{i=0}^{N-1} (\mathrm{z}_{i|k}^T Q \mathrm{z}_{i|k} + \mathrm{v}_{i|k}^T R \mathrm{v}_{i|k}) + \mathrm{z}_{N|k}^T P \mathrm{z}_{N|k}, \tag{33}$$

and the related finite horizon optimal control problem can be reformulated.

The solution of the optimization problem is the optimal nominal control sequence $\mathbf{v}_{0|k}(\mathrm{z})$. The optimal control applied to the nominal system is the first control action of this sequence, i.e., $\tilde{\kappa}_N(\mathrm{z}) := \mathrm{v}_k^0(0; \mathrm{z}_k)$. The control strategy applied to the uncertain system, according to the adopted feedback policy, is

$$\kappa_N(\mathrm{x}_k, \mathrm{z}_k) = \tilde{\kappa}_N(\mathrm{z}_k) + K(\mathrm{x}_k - \mathrm{z}_k). \tag{34}$$

The closed-loop system then satisfies

$$\begin{aligned} \mathrm{x}_{i+1|k} &= A_d \mathrm{x}_{i|k} + B_d \kappa_N(i, \mathrm{x}_k, \mathrm{z}_k) + B_{w_d} \mathrm{w}_{i|k}, \\ z_{i+1|k} &= A_d \mathrm{z}_{i|k} + B_d \tilde{\kappa}_N(i, \mathrm{z}_k). \end{aligned} \tag{35}$$

In [43], this robust MPC is compared in terms of computational cost, fuel consumption, and constraints satisfaction with a classical MPC, based on linear-quadratic (LQ) MPC, when the system is affected by persistent bounded uncertainties. On one side, the classical MPC allows real-time implementation ensuring stability with a reasonable computational effort.

Starting from the approach proposed in [58], the authors of [43] evaluated the performance of the tube-based MPC within the space rendezvous scenario both in simulations, in which a three DoF orbital simulator is considered, and in an experimental setup. Hence, the TRMPC effectiveness of a real-time implementation on a spacecraft is already verified. A reasonable computational effort for the robust approach, as clearly explained in [43], is obtained with a time-varying control law where the feedback gain matrix is evaluated offline. As verified in [43], the use of a linear-matrix-inequality (LMI) method improves the computational efficiency of robust MPC even when using low-thrust propulsion.

5.4 Stochastic Model Predictive Control

MPC offers a certain degree of robustness to system uncertainties due to its receding-horizon implementation.

As discussed in the Introduction, in the classical approaches, orbital perturbations, disturbances, and model errors are not taken into account. For this reason in [44] the authors presented a real-time stochastic model predictive control (SMPC), in which autonomous docking is achieved. The reasons behind this research are the development of a controller able to perform the docking between the chaser and the target, in a safe way and in an experimental setup. The choice of adopting a stochastic approach instead of robust MPC ones is motivated by the fact that the type of uncertainties typically encountered in the ARVD operations in general have a probabilistic description, and that the trajectory constraints imposed to the spacecraft may indeed allow a probability of violation, in trade of a better performance.

The novelties of the approach proposed in [44] are: (i) from the theoretical point of view, both parametric uncertainties and additive disturbances are included, (ii) from the experimental point of view, the proposed experimental setup allows the computational effort largely to be reduced with respect to other SMPC techniques, thanks to the offline evaluation of the feedback gain matrix. Moreover, a realistic model (based on the experimental setup described in Section 6), which takes into account both external disturbances and uncertainties due to variations of the spacecraft parameters during the flight and to model linearization, is included.

From a theoretical viewpoint, the approach in [44] is based on the works [45] and [46], extending the results by considering the simultaneous presence of parametric uncertainties and of the additive noise, modeled in accordance to an experimental

Fig. 5 NPS-POSEIDYN testbed with the Vicon motion capture cameras, FSSs, and granite monolith in the Spacecraft Robotics Laboratory at the Naval Postgraduate School. The target FSS is on the right and the chaser FSS is on the left.

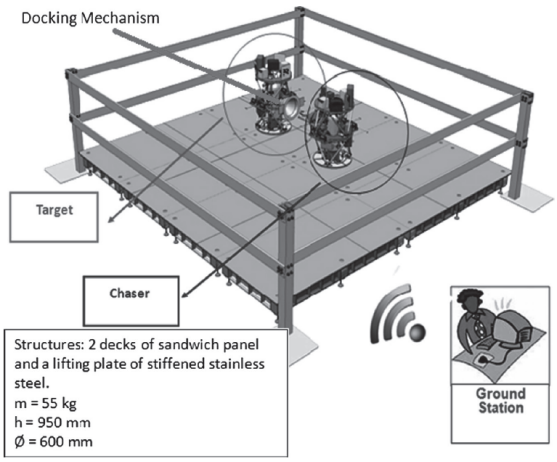

Fig. 6 The experimental rig: chaser (right) and target (left).

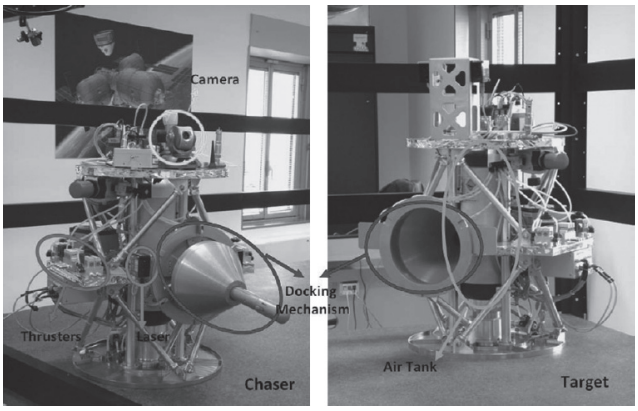

Fig. 7 The rendezvous experimental rig: chaser and target vehicles.

setup. It should be remarked that the approach proposed in [44] shares all the attractive features of [45] and [46]. First, the sampling is performed offline, thus allowing to reduce the online computational cost of the algorithm. This allows to largely mitigate the potential drawback of sampling-based SMPC methods, related to the high online computational cost, as clearly explained in [60],[61], which may render these approaches not easily implementable in real applications.

6. Simulation and Experimental Models

To assess the goodness and applicability of a GNC scheme, a key role is played by software simulations and experimental test-beds. To design a flight software as close as possible to a "flyable" format, a six degree-of-freedom (six DoF) orbital simulator is usually considered. For "flyable" verification of the GNC system in simulation, a local connection, in which the six DoF simulator is the server and the GNC system is the client, is adopted. The simulator sends sensor data to the GNC system and the GNC sends the inputs data to the actuation systems. In this way, a two-channel segment is considered, as explained before, as in the case of real space software, in which the space segment includes the guidance and control system and the ground segment has simulators and flight dynamics systems.

In this section, we briefly describe two different testbeds where the discussed algorithms have been tested: (i) a three DoF testbed in the the Naval Postgraduate School (NPS) of Monterey [62], and (ii) a three DoF testbed in Thales Alenia Space, Turin [63]. For obvious reasons, both testbeds can analyze only the proximity maneuver.

The testbed at NPS is called POSEIDYN – Proximity Operation of Spacecraft: Experimental hardware-In-the-loop DYNnamic simulator, and it consists of floating spacecraft simulators (FSS), a polished granite monolith, a Vicon motion capture system, and a ground station computer. Figure 5 shows an overview of the testbed. The floating surface is a 15 t, 4-m-by-4 m granite monolith, with a planar accuracy of ±0.0127 mm and a horizontal leveling accuracy of less than 0.01°. The FSSs float over the granite surface via three flat air bearings. The quasi-frictionless environment with the low residual acceleration of the FSS emulates the environment in space. The FSS has eight cold gas thrusters fed by compressed air from an on-board tank [64]. Using the on-board computer, the FSS is able to perform real-time computation of guidance and control algorithms.

The second testbed we briefly describe was developed in the frame of STEPS (systems and technologies for space exploration) program, which was a project co-financed by Regione Piemonte (Piedmont Region) within the P.O.R.-F.E.S.R. 2007-2013 EC program [63]. The vehicles float using a thin air film of 60 μm over a very flat floor, which produces a nearly frictionless environment in planar dynamic with three DoF (Figs. 6 and 7). The target vehicle is supposed to keep on moving on a predefined trajectory, while the chaser vehicle has full maneuver capabilities. Vehicles motion is controlled by 14 cold gas actuators with three different levels of thrust.

7. Conclusions

This paper presented an overview of GNC computational-efficient algorithms for real time applications in space. The distinguishing feature of the presented approaches are related to the combination of different guidance and control algorithms for a complete space maneuver, in which the controller design is focused on a real application: (1) reduced frequency of the controller for fuel saving, (2) pulse width modulation of thrusters and (3) realistic actuator models.

References

[1] B.C. Hacker: On the shoulders of Titans: A history of Project Gemini, *NASA Technical Report*, NASA-SP-4203, 1977.

[2] K.A. Young and J.D. Alexander: *Apollo lunar rendezvous*, American Institute of Aeronautics and Astronautics, 1970.

[3] J. Fabrega, M. Frezet, and J.L. Gonnaud: ATV GNC during rendezvous, *Spacecraft Guidance, Navigation and Control Systems*, Vol. 381, pp. 85–93, 1997.

[4] S. Ueda, K. Toru, and H. Uematsu: HTV rendezvous technique and GNC design evaluation based on 1st flight on-orbit operation result, *AIAA/AAS Astrodynamics Specialist Conference*, pp. 1–12, 2010.

[5] R. Hall and D. Shayler: *Soyuz: A universal spacecraft*, Springer Science & Business Media, 2003.

[6] P. Miotto, L. Breger, I. Mitchell, B. Keller, and B. Richikot: Designing and validating proximity operations rendezvous and approach trajectories for the cygnus mission, *AIAA Guidance, Navigation, and Control Conference*, pp. 1–18, 2010.

[7] M. Jones, E. Gomez, A. Mantineo, and U.K. Mortensen: *Introducing ECSS Software-Engineering Standards within ESA*, EASA bulletin, 2002.

[8] Y. Luo, J. Zhang, and G. Tang: Survey of orbital dynamics and control of space rendezvous, *Chinese Journal of Aeronautics*, Vol. 27, No. 1, pp. 1–11, 2014.

[9] L. Holguin, S. Prabhakaran Viswanathan, and A. Sanyal: Guidance and control for spacecraft autonomous rendezvous and proximity maneuvers using a geometric mechanics framework, *AIAA Guidance, Navigation, and Control Conference*, pp. 1–14, 2012.

[10] L. Sun and W. Huo: Robust adaptive control of spacecraft proximity maneuvers under dynamic coupling and uncertainty, *Advances in Space Research*, Vol. 56, pp. 2206–2217, 2015.

[11] S.J. Maclellan: *Orbital Rendezvous Using an Augmented Lambert Guidance Scheme*, Master Thesis, MIT, 2005.

[12] J.L. Goodman: History of space shuttle rendezvous and proximity operations, *Journal of Spacecraft and Rockets*, Vol. 43, No. 5, pp. 944–959, 2006.

[13] A.R. Tatsch and N. Fitz-Coy: Dynamic artificial potential function guidance for autonomous on-orbit servicing, *6th International ESA Conference on Guidance, Navigation and Control Systems*, Loutraki, Greece, ESA SP-606, 2005.

[14] N. Martinson: Obstacle avoidance guidance and control algorithm for spacecraft maneuvers, *AIAA Guidance, Navigation, and Control Conference*, pp. 1–9, 2009.

[15] W. Fehse: *Automated Rendezvous and Docking of Spacecraft*, Cambridge University Press, 2003.

[16] P. Betsch and R. Siebert: Rigid body dynamics in terms of quaternions: Hamiltonian formulation and conserving numerical integration, *International Journal for Numerical Methods in Engineering*, Vol. 79, No. 4, pp. 444–473, 2009.

[17] K. Yamanaka and F. Ankersen: New state transition matrix for relative motion on an arbitrary elliptical orbit, *Journal of Guidance, Control and Dynamics*, Vol. 25, No. 1, pp. 60–66, 2002.

[18] G. Avanzini: A simple Lambert algorithm, *Journal of Guidance, Control and Dynamics*, Vol. 31, No. 6, pp. 1587–1594, 2008.

[19] D. Vallado: *Fundamentals of Astrodynamics and Applications*, Microcosm Press, 2007.

[20] M.G. Yoon: Relative circular navigation guidance for three-dimensional impact angle control problem, *Journal of Aerospace Engineering*, Vol. 33, No. 4, pp. 300–308, 2010.

[21] A.E. Bryson and Y.C. Ho: *Applied Optimal Control: Optimization, Estimation, and Control*, Wiley, 1975.

[22] P. Zarchan: *Tactical and Strategic Missile Guidance*, Progress in Astronautics and Aeronautics, 2012.

[23] M. Hawkins: *New near-optimal feedback guidance algorithms*, PhD Dissertation, Iowa State University, 2013.

[24] M. Hawkins, Y. Guo, and B. Wie: Spacecraft guidance algorithms for asteroid intercept and rendezvous, *International Journal of Aeronautical and Space Science*, Vol. 13, No. 2, pp. 154–169, 2012.

[25] J. Guldner and V.I. Utkin: Sliding mode control for gradient tracking and robot navigation using artificial potential fields, *IEEE Transactions on Robotics and Automation*, Vol. 11, No. 2, pp. 247–254, 1995.

[26] M. Mammarella, E. Capello, and G. Guglieri: A comprehensive analysis of guidance and control algorithms for orbital rendezvous maneuvers, *AIAA SPACE and Astronautics Forum and Exposition 2016*, pp. 1–11, 2016.

[27] M. Dentis, E. Capello, and G. Guglieri: A novel concept for guidance and control of spacecraft orbital maneuvers, *International Journal of Aerospace Engineering*, Vol. 2016, pp. 1–14, 2016.

[28] N. Bloise, E. Capello, M. Dentis, and E. Punta: Obstacle avoidance with potential field applied to a rendezvous maneuver, *Applied Sciences*, Vol. 7, No. 10, 1042, pp. 1–16, 2017.

[29] A. Ferrara and M. Rubagotti: Second-order sliding-mode control of a mobile robot based on a harmonic potential field, *IET Control Theory and Applications*, Vol. 2, No. 9, pp. 807–818, 2008.

[30] D. Fu-guang, J. Peng, B. Xin-qian, and W. Hong-jian: AUV local path planning based on virtual potential field, *IEEE International Conference on Mechatronics and Automation*, Vol. 4, pp. 1711–1716, 2005.

[31] J. Kosecka: *Potential Field Methods*, Technical Report, GMU CS Department, 2017.

[32] P.C. Hughes: *Spacecraft Attitude Dynamics*, Dover Publications, 2004.

[33] J. Jie, Y. Yu, and M. Kemao: Continuous optimal terminal proximity guidance algorithm for autonomous rendezvous and docking, *Information Technology Journal*, Vol. 12, pp. 1011–1017, 2013.

[34] D.T. Stansbery and J.R. Cloutier: Position and attitude control of a spacecraft using the state-dependent Riccati equation technique, *Proceedings of the American Control Conference*, pp. 1867–1871, 2000.

[35] D. Lee, J. Cochran Jr., and T. No: Robust position and attitude control for spacecraft formation flying, *Journal of Aerospace Engineering*, Vol. 25, No. 3, pp. 436–447, 2012.

[36] J. Lyu, J. Qin, Q. Ma, W.X. Zheng, and Y. Kang: Finite-time attitude synchronization for multiple spacecraft, *IET Control Theory and Applications*, Vol. 10, No. 10, pp. 1106–1114, 2016.

[37] K. Subbarao and S. Welsh: Nonlinear control of motion synchronization for satellite proximity operations, *Journal of Guidance, Control, and Dynamics*, Vol. 31, No. 5, pp. 1284–1294, 2008.

[38] S. Di Cairano, H. Park, and I. Kolmanovsky: Model predictive control approach for guidance of spacecraft rendezvous and proximity maneuvering, *International Journal of Robust and Nonlinear Control*, Vol. 22, No. 12, pp. 1398–1427, 2012.

[39] M. Leomanni, E. Rogers, and S.B. Gabriel: Explicit model predictive control approach for low-thrust spacecraft proximity operations, *Journal of Guidance, Control, and Dynamics*, Vol. 37, No. 6, pp. 1780–1790, 2014.

[40] A. Weiss, M. Baldwin, R.S. Erwin, and I. Kolmanovsky: Model predictive control for spacecraft rendezvous and docking: Strategies for handling constraints and case studies, *IEEE Transactions on Control Systems Technology*, Vol. 23, No. 4, pp. 1638–1647, 2015.

[41] E. Capello, E. Punta, F. Dabbene, G. Guglieri, and R. Tempo: Sliding mode control strategies for rendezvous and docking maneuvers, *Journal of Guidance, Control and Dynamics*, Vol. 40, No. 6, pp. 1481–1487, 2017.

[42] E. Capello, E. Punta, and G. Bartolini: Simplex sliding mode control strategies for spacecraft rendezvous maneuvers, *IFAC PapersOnLine*, Vol. 50, pp. 8496–8501, 2017.

[43] M. Mammarella, E. Capello, H. Park, G. Guglieri, and M. Romano: Spacecraft proximity operations via tube-based robust model predictive control with additive disturbances, *68th International Astronautical Congress*, IAC17C1.5.3.x37611, 2017.
[44] M. Mammarella, E. Capello, M. Lorenzen, F. Dabbene, and F. Allgöwer: A general sampling-based SMPC approach to spacecraft proximity operations, *56th IEEE Conference on Decision and Control*, Melbourne, Australia, 2017.
[45] M. Lorenzen, F. Allgöwer, F. Dabbene, and R. Tempo: Stochastic MPC with offline uncertainty sampling, *Automatica*, Vol. 81, pp. 176–183, 2017.
[46] M. Lorenzen, F. Dabbene, R. Tempo, and F. Allgöwer: Constraint-tightening and stability in stochastic model predictive control, *IEEE Transactions on Automatic Control*, Vol. 62, No. 7, pp. 3165–3177, 2017.
[47] R. Bevilacqua, T. Lehmann, and M. Romano: Development and experimentation of LQR/APF guidance and control for autonomous proximity maneuvers of multiple spacecraft, *Acta Astronautica*, Vol. 68, No. 7, pp. 1260–1275, 2011.
[48] L. Walker: Automated proximity operations using image-based relative navigation, *26th Annual USU/AIAA Conference on Small Satellites*, SSC12-VIII-3, 2012.
[49] B. Ebrahimi, M. Bahrami, and J. Roshanian: Optimal sliding-mode guidance with terminal velocity constraint for fixed-interval propulsive maneuvers, *Acta Astronautica*, Vol. 62, No. 10-11, pp. 556–562, 2008.
[50] S.S. Shamshirgar, M. Golkhah, H. Rahmati, and M.A. Nekoui: Application and comparison of LQR and robust sliding mode controllers to improve power system stability, *Environmental and Electrical Engineering International Conference*, pp. 10–13, 2009.
[51] V.I. Utkin: *Sliding Modes in Optimization and Control Problems*, Springer, 1992.
[52] G. Bartolini, A. Ferrara, and E. Usai: Chattering avoidance by second-order sliding mode control, *IEEE Transactions on Automatic Control*, Vol. 43, No. 2, pp. 241–246, 1998.
[53] A. Levant: Sliding order and sliding accuracy in sliding mode control, *International Journal of Control*, Vol. 58, No. 6, pp. 1247–1263, 1993.
[54] W.J. Cao and J.X. Xu: Nonlinear integral-type sliding surface for both matched and unmatched uncertain systems, *IEEE Transactions on Automatic Control*, Vol. 49, No. 8, pp. 1355–1360, 2004.
[55] F. Castanos and L. Fridman: Analysis and design of integral sliding manifolds for systems with unmatched perturbations, *IEEE Transactions on Automatic Control*, Vol. 51, No. 5, pp. 853–858, 2006.
[56] S. Mondal, T.V. Gokul, and C. Mahanta: Adaptive second order sliding mode controller for vertical take-off and landing aircraft system, *IEEE 7th International Conference on Industrial and Information Systems*, Chennai, India, 2012.
[57] B. Kouvaritakis and M. Cannon: Model predictive control: Classical, robust and stochastic, *Advanced Textbooks in Control and Signal Processing*, Springer, 2015.
[58] D.Q. Mayne and J.B. Rawlings: *Model Predictive Control: Theory and Design*, Nob Hill Publishing, 2009.
[59] S.V. Rakovic and D.Q. Mayne: A simple tube controller for efficient robust model predictive control of constrained linear discrete time systems subject to bounded disturbances, *IFAC Proceedings Volumes*, Vol. 38, No. 1, pp. 241–246, 2005.
[60] A. Mesbah: Stochastic model predictive control: An overview and perspectives for future research, *IEEE Control Systems*, Vol. 36, No. 6, pp. 30–44, 2016.
[61] L. Blackmore, M. Ono, A. Bektassov, and B.C. Williams: A probabilistic particle-control approximation of chance-constrained stochastic predictive control, *IEEE Transactions on Robotics*, Vol. 26, No. 3, pp. 502–517, 2010.
[62] R. Zappulla II, J. Virgili-Llop, C. Zagaris, H. Park, and M. Romano: Dynamic air-bearing hardware-in-the-loop testbed to experimentally evaluate autonomous spacecraft proximity maneuvers, *Journal of Spacecraft and Rockets*, Vol. 54, No. 4, pp. 825–839, 2017.
[63] G. Guglieri, F. Maroglio, P. Pellegrino, and L. Torre: Design and development of guidance navigation and control algorithms for spacecraft rendezvous and docking experimentation, *Acta Astronautica*, Vol. 94, No. 1, pp. 395–408, 2014.
[64] C. Lugini and M. Romano: A ballistic-pendulum test stand to characterize small cold-gas thruster nozzles, *Acta Astronautica*, Vol. 64, pp. 615–625, 2009.

Elisa Capello

She received his B.S., M.S., and Ph.D. degrees from Politecnico di Torino, in 2003, 2006, 2011, respectively. She is currently an Assistant Professor of the Department of Mechanical and Aerospace Engineering. She is a Research Associate of CNR IEIIT. Her research interests include control systems design, flight mechanics, space and aerial systems. She is a member of IEEE.

Fabrizio Dabbene

He received the M.S degree in 1995 and the Ph.D. degree in 1999, from Politecnico di Torino, Italy. He is currently Senior Researcher at the CNR-IEIIT institute. His research interests include randomized and robust methods for systems and control, with applications to aerospace, environmental systems and energy. He served as Associate Editor for Automatica (2008–2014) and for the IEEE Transactions on Automatic Control (2008–2012). He is a Senior Member of the IEEE, and served as elected member of the IEEE-CSS Board of Governors (2014–2016) and as IEEE-CSS Vice President for Publications (2015-2016).

Giorgio Guglieri

He received his M.S. degrees from Politecnico di Torino in 1989. He is currently a Full Professor of Politecnico di Torino in the Department of Mechanical and Aerospace Engineering. His research interests include flight mechanics, unmanned aerial vehicles and space systems. He is Senior Member AIAA and Member AHS.

Elisabetta Punta

She received her M.S. in Electronic Engineering and Ph.D. in Electronic Engineering and Computer Science degrees from University of Genoa, Italy, in 1993 and 1998, respectively. In 2003 she joined the National Research Council of Italy (CNR), where she is currently a Researcher of the Institute IEIIT of CNR. Her research interests include nonlinear control systems and observers design. She is a Senior Member of IEEE.